INDEX COPERNICUS INTERNATIONAL

Bio-Algorithms and Med-Systems

WWW.BAMSJOURNAL.COM ISSN: 1896-530X

Exploration of simultaneous dual--isotope imaging with a multiphoton modular J-PET scanner

Ermias Y. Beyene[1,2,3,4ABCDEF] (ORCID: 0009-0002-8757-2169), Manish Das[3,4B] (ORCID: 0009-0001-2901-1745), Martyna Durak-Kozica[3,4B] (ORCID: 0000--0002-5275-6462), Grzegorz Korcyl[3,4B] (ORCID: 0000-0001-6244-7287), Wiktor Mryka[3,4B] (ORCID: 0009-0006-7616-8290), Szymon Niedźwiecki[3,4BD] (ORCID: 0000-0002-5953-9479), Szymon Parzych[3,4BC], Keyvan Tayefi[3,4B] (ORCID: 0000-0001-8764-1588), Rafał Walczak[5B] (ORCID: 0000-0002--0308-7223), Kamil Wawrowicz[3,4B] (ORCID: 0000-0003-3818-5840), Ewa Stepien[3,4ADEFG] (ORCID: 0000-0003-3589-1715), Pawel Moskal[3,4ABCDEFG] (ORCID: 0000-0002-4229-3548), on behalf of J-PET collaboration

[1]Doctoral School of Exact and Natural Science, Jagiellonian University, Krakow, Poland
[2]Department of Experimental Particle Physics and Applications, Jagiellonian University in Krakow, Krakow, Poland
[3]Faculty of Physics, Astronomy and Applied Computer Science, Jagiellonian University, Krakow, Poland
[4]Centre for Theranostics, Jagiellonian University, Krakow, Poland
[5]Institute of Nuclear Chemistry and Technology, Centre of Radiochemistry and Nuclear Chemistry, Warsaw, Poland

ABSTRACT

The modular J-PET scanner, comprising 24 compact and versatile modules, each consisting of 13 plastic strips with four SiPM detectors at the ends, represents a powerful tool for clinical applications in nuclear medical imaging. This study presents preliminary results from the exploration of simultaneous dual-isotope imaging using the modular J-PET system. Our approach involved two isotopes: ^{68}Ge, characterized by a ringlike shape, and ^{22}Na, exhibiting a point-like shape. The imaging was based on double-coincidence and triple-coincidence events. In the double coincidence case, both isotopes contributed comparably, whereas in the triple coincidence case ^{22}Na dominated due to the prompt gamma being emitted with 100% of positron emissions, unlike ^{68}Ga, where the prompt gamma was emitted in only 1.3% of cases after positron emission. In this work we present direct 2γ images determined for two-signal events and images for three-signal events, with two signals from annihilation photons and one from a prompt gamma. These results showcase the preliminary findings from simultaneous dual-isotope imaging of ^{68}Ga and ^{22}Na isotopes using the modular J-PET scanner, which will be presented and discussed.

KEYWORDS

Dual isotope imaging, $\beta^+ + \gamma$ imaging, 2γ imaging, medical imaging, J-PET, PET, multiphoton PET

ORIGINAL ARTICLE

Received: 13.12.2023
Accepted: 25.12.2023
Published: 31.12.2023

CITE THIS ARTICLE AS:
Beyene EY, Das M, Durak--Kozica M, Korcyl G, Mryka W, Niedzwiecki S, Parzych S, Tayefi K, Walczak R, Wawrowicz K, Stepien E, Moskal P, on behalf of J-PET collaboration, "Exploration of simultaneous dual-isotope imaging with a multiphoton modular J-PET scanner," Bio-Algorithms and Med-Systems vol. 1, no. 1, pp. 101-108, 2023, DOI: 10.5604/01.3001.0054.1940

AUTHORS' CONTRIBUTION:
A – Study Design
B – Data Collection
C – Statistical Analysis
D – Data Interpretation
E – Manuscript Preparation
F – Literature Search
G – Funds Collection

CORRESPONDING AUTHOR:
Ermias Y. Beyene (ORCID: 0009-0002-8757-2169); Doctoral School of Exact and Natural Science, Jagiellonian University, Kraków, Poland; Łojasiewicza street 11, 30-348 Kraków, Poland; E-mail: ermiasyitayew.beyene@doctoral.uj.edu.pl

LIST OF ABBREVIATIONS

J-PET – Jagiellonian Positron Emission Tomography
mV – millivolt
PET – Positron Emission Tomography
Ps – picosecond
ST – scatter test
TOF – time of flight
TOT – time over threshold
ns – nanosecond

INTRODUCTION

The modular Jagiellonian Positron Emission Tomography (J-PET) detector represents an innovative and cost-effective prototype for a PET system utilizing plastic scintillators [1–4]. What sets the modular J-PET detector apart is its unique capability for multiphoton registration with triggerless data acquisition [5], coupled with its cost-effectiveness and portability. These features render it a valuable tool across a spectrum of medical applications, encompassing standard PET [4], positronium imaging [1, 6–12], multiphoton imaging [1, 13], dual-isotope PET imaging and simultaneous multi-molecule and inter-molecule imaging [14–17]. J-PET also finds applications in basic research of positronium decays [13, 18] and proton-beam-therapy monitoring [19].

The scanner comprises 24 modules, each housing 13 scintillators equipped with four silicon photomultiplier detectors on each side. This detector system ensures robust and reliable signal detection [1–3]. Its technology maintains a compact form factor, weighing only 60 kg and boasting a diameter of 76.2 cm [1, 2]. Furthermore, the system offers an expansive field of view (FOV) spanning 50 cm, with each scintillator's cross-section measuring 6 mm × 24 mm [1, 20].

The triggerless mode introduces flexibility in event selection, enabling the registration and identification of two- and three--photon annihilation events, along with prompt gammas emitted by isotopes known as $\beta^+ + \gamma$ emitters [1, 8, 21, 22]. Ongoing efforts addressing challenges such as crosstalk aim at the full implementation of multi-molecule and inter-molecule imaging. In this context, J-PET emerges as a promising alternative in the dynamic field of nuclear medicine [1, 14].

In conventional PET imaging, 2γ (two-photon) coincidence events have long been the clinical standard, offering invaluable insights into various medical conditions [1, 23, 24]. This includes the diagnosis and monitoring of cancers using radiotracers such as fluorodeoxyglucose (FDG) in oncology, cardiovascular disease assessment and neuroimaging for studying brain function [25, 26].

Recent advancements, however, have expanded imaging capabilities to encompass multiphoton coincidence events and $\beta^+ + \gamma$ imaging [1, 6, 9, 13]. Suitable candidates for $\beta^+ + \gamma$ imaging include ^{22}Na, ^{44}Sc, ^{72}As, ^{60}Cu, ^{10}C, ^{14}O, ^{34}Cl, ^{48}V, ^{52}Mn, ^{55}Co, ^{60}Cu, ^{66}Ga, ^{69}Ga, ^{76}Br, ^{82}Rb, ^{86}Y, ^{94}Tc, ^{110}In, ^{124}I [1, 14, 16, 22, 27], and β^+ emitters such as ^{18}F, ^{15}O, ^{11}C, ^{89}Z, ^{64}Cu, ^{13}N [14, 22, 27].

In this article, by utilizing the J-PET scanner we investigate the possibility of simultaneous 2γ and 2γ + prompt events in PET imaging. These investigations are conducted using two distinct isotopes, ^{22}Na and ^{68}Ge, which exhibit comparable activity. Despite their similarities, these isotopes differ significantly in terms of half--lives, decay pathways and nuclear characteristics, as illustrated in Fig. 1.

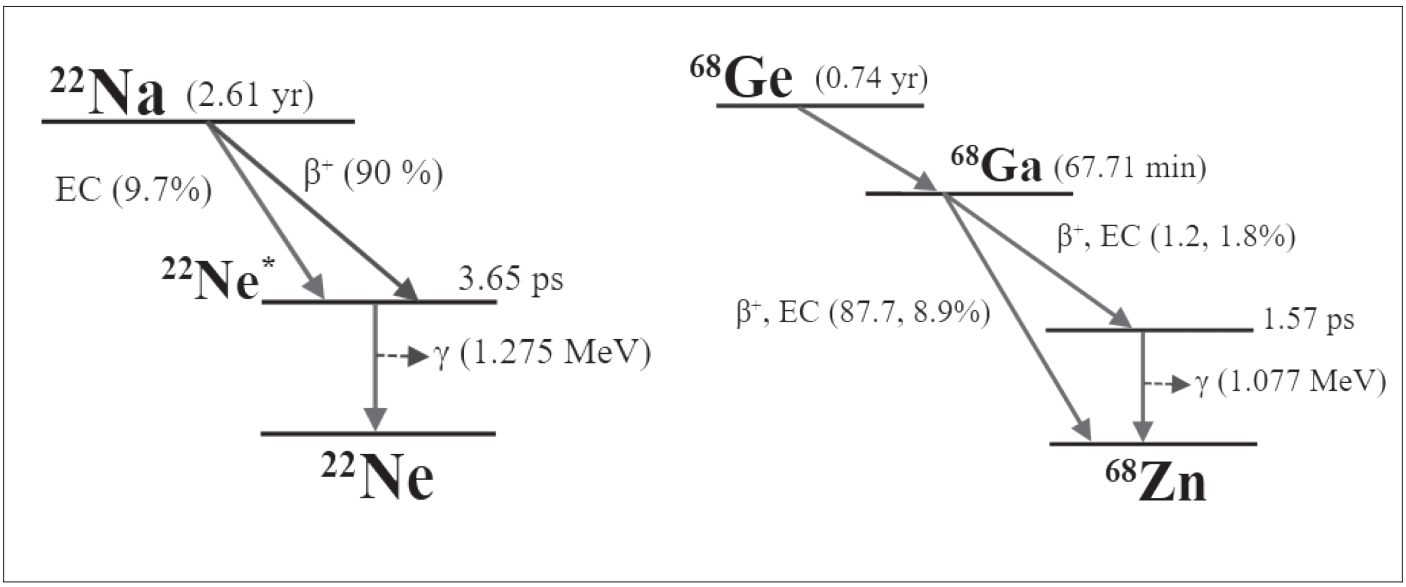

Fig. 1. Decay schemes of ^{22}Na and ^{68}Ge, which are used for this measurement. Here, EC denotes electron capture; β^+ is positron emission, including the branching ratio; γ is the deexcitation process, providing information on its energy and lifetime.

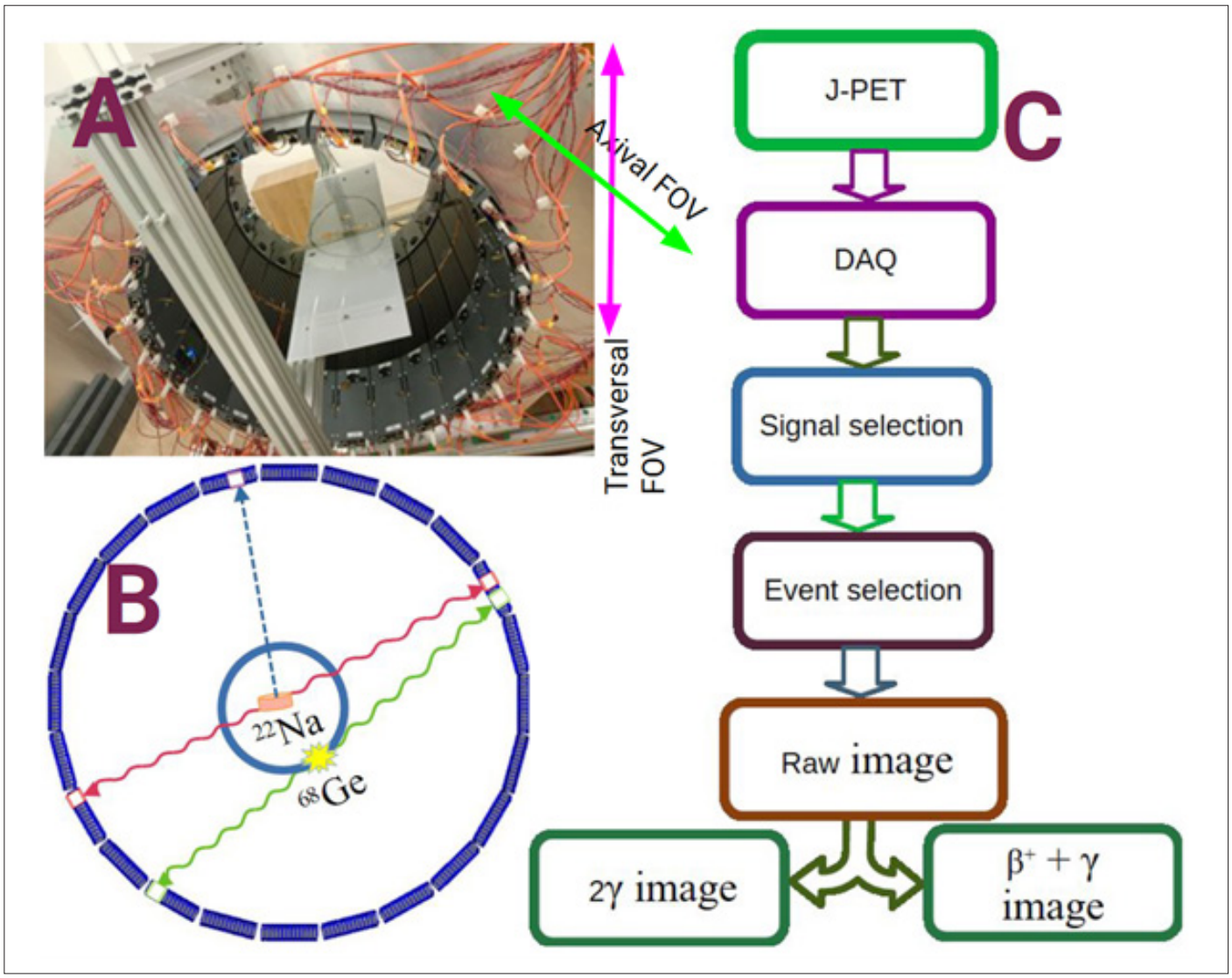

Fig. 2. (A) The photograph showing the setup of the measurement with the sources, the carbonate plate in the 24 modular J-PET scanner; (B) the schematic cross-section of the 24 modular J-PET with the pictorial illustration of the putative annihilation and prompt gamma (dashed arrow). The point-like ^{22}Na source (red) is placed close to the centre and the ^{68}Ge germanium source forms a ring, shown in blue, and the registration of photons is marked with a white spot; (C) Data processing scheme including: data acquisition (DAQ), signal selection and event filtering, culminating in the transformation to raw 2γ and $\beta^+ + \gamma$ images.

METHODS

The study started with the experimental setup by first enclosing the ^{68}Ge source within a 0.6-mm thick aluminium casing and secured with a four-loop (0.6 × 4 mm = 2.4 mm) standard aluminium foil. The 70-cm ^{68}Ge line source was then configured into a ringlike shape to facilitate our dual-isotope imaging endeavours. Simultaneously, we introduced the metallic ^{22}Na source into the setup with a point-like configuration. The ^{68}Ge source possessed an activity of 1.699 MBq, while the ^{22}Na source exhibited an activity of 1.633 MBq. These isotopes were positioned at different locations within the detector, and data collection commenced to enable simultaneous registration of signals from the two isotopes.

To ensure the stable placement of the sources within the detector we employed a rectangular carbonate plate. This carbonate plate offered stability and also guaranteed positioning of the sources within the detector, as shown in Fig. 2A.

After completing the data collection phase, our analytical focus expanded to cover both 2γ (two-hit) and $\beta^+ + \gamma$ (three-hit) scenarios. In the 2γ (double coincidence) case, both isotopes made comparable contributions, while in the $\beta^+ + \gamma$ (triple coincidence) scenario, ^{22}Na played a significant role due to the inherent association of every β^+ emission with a prompt gamma. Notably, in this analysis we neglected the contribution of the prompt gamma from the germanium ring, primarily due to its low branching ratio. The regions selected for images are two- and three-hit events,

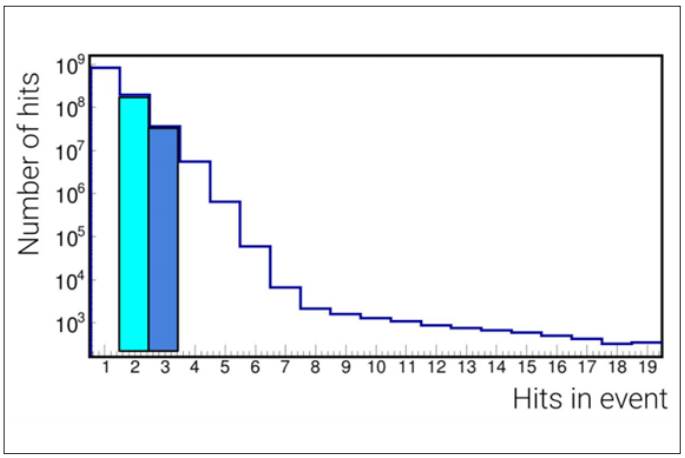

Fig. 3. The multiplicity of hits within a single event, with the shaded regions denoting multiplicity of two (cyan rectangular box) and three (blue rectangular box) hits. For the annihilation-point reconstruction, the signals from two annihilation gamma are used and the annihilation place is reconstructed using the GKDE method [28, 29]. Signals from annihilation photons and prompt gamma are identified based on the TOT measurement, a measure of energy deposition to the detector [30].

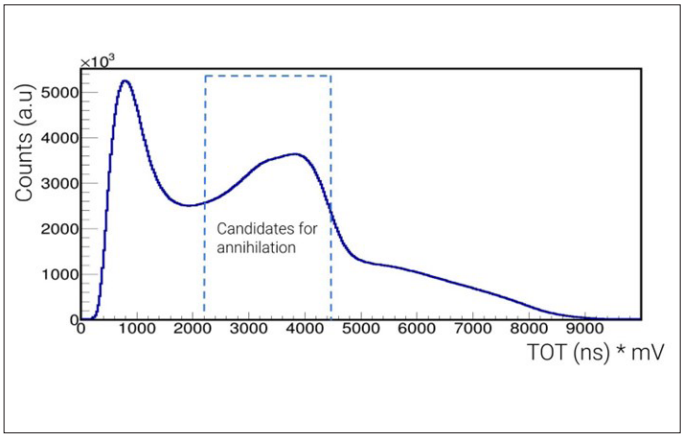

Fig. 4. TOT plot for two-hit events, showing the energy deposition. The upper limit of the selected region corresponds to the Compton edge from 511 keV annihilation photons.

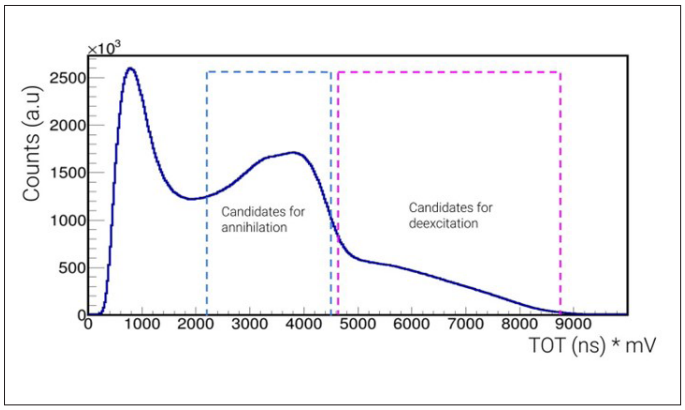

Fig. 5. TOT plot for three-hit events.The selected regions correspond to the upper half of spectrum from Compton edge from 511 keV annihilation photons, and the part of the spectrum for large TOT values is due to the prompt gamma (from 1275 keV photons).

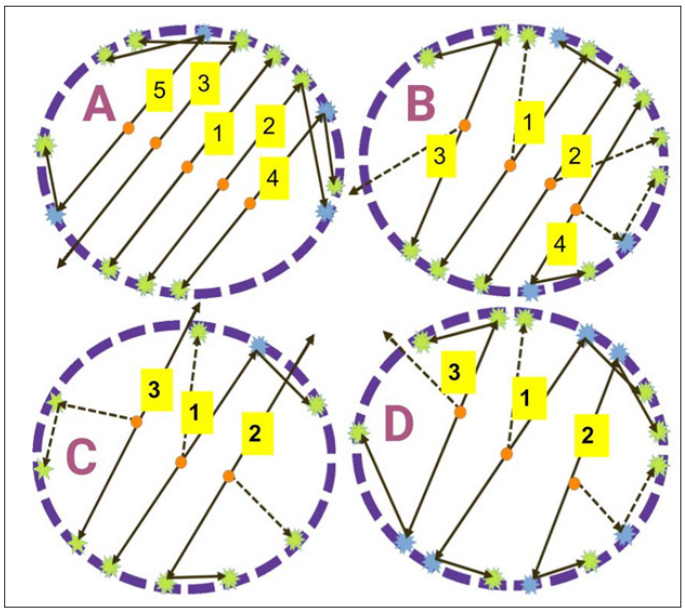

Fig. 6. Pictorial representation of scatterings happening in the detector. The green star represents deposited energy within the identification window, while the blue star indicates signals with TOT below the annihilation window. It includes: (A) Case 1: true coincidence, where both photons from an annihilation event are detected by detectors. Case 2: represents a scenario of true coincidence, but in this case one of the photons scatters and the scattered photon has insufficient energy to be detected in the TOT range. Case 3: depicts a situation in which one of the photons goes undetected while the other photon generates two signals, one before and the other after it scatters. Case 4: shows a scenario in which one of the gamma rays is registered without scattering and the other is registered after scatter. Case 5: represents an event in which both of the annihilation photons scatter and are detected after scattering; (B) Case 1: represents three-hit events, denotes the triple coincidence case from three-hit-event size. Case 2: depicts a scenario in which one of the annihilation gamma rays scatters but does not produce signals after scattering, while the other annihilation gamma and the prompt gamma are detected. Case 3: represents a case in which three signals come from the annihilation photons. One of the annihilation photons scatters and produces two signals, while the other is not scattered but is registered. In this scenario, the deexcitation gamma is not detected. Case 4: depicts a situation in which the deexcitation gamma and one of the annihilation photons scatter, and the scatters are detected. Meanwhile, the other annihilation photon is detected with no scattering; (C) Case 1: depicts a scenario in which one of the annihilation gamma rays scatters and the scattered one is detected. Case 2: shows a situation in which one of the annihilation gamma rays is not detected but the other annihilation gamma scatters, producing two signals, before and after scattering. Case 3: represents a case in which one of the annihilation photons is not registered, but the deexcitation gamma scatters and produces two signals before and after scattering. Additionally, one of the annihilation gamma rays is detected before it scatters; (D) Case 1: represents a scenario in which three signals originate from annihilation and deexcitation events. In this case, both of the annihilation photons scatter and are detected after scattering, and the deexcitation gamma is also detected. Case 2: depicts a case in which all three hits are scattered and produce signals after scattering. Case 3: shows a situation in which the annihilation photons produce three signals after scattering and the deexcitation gamma is not detected.

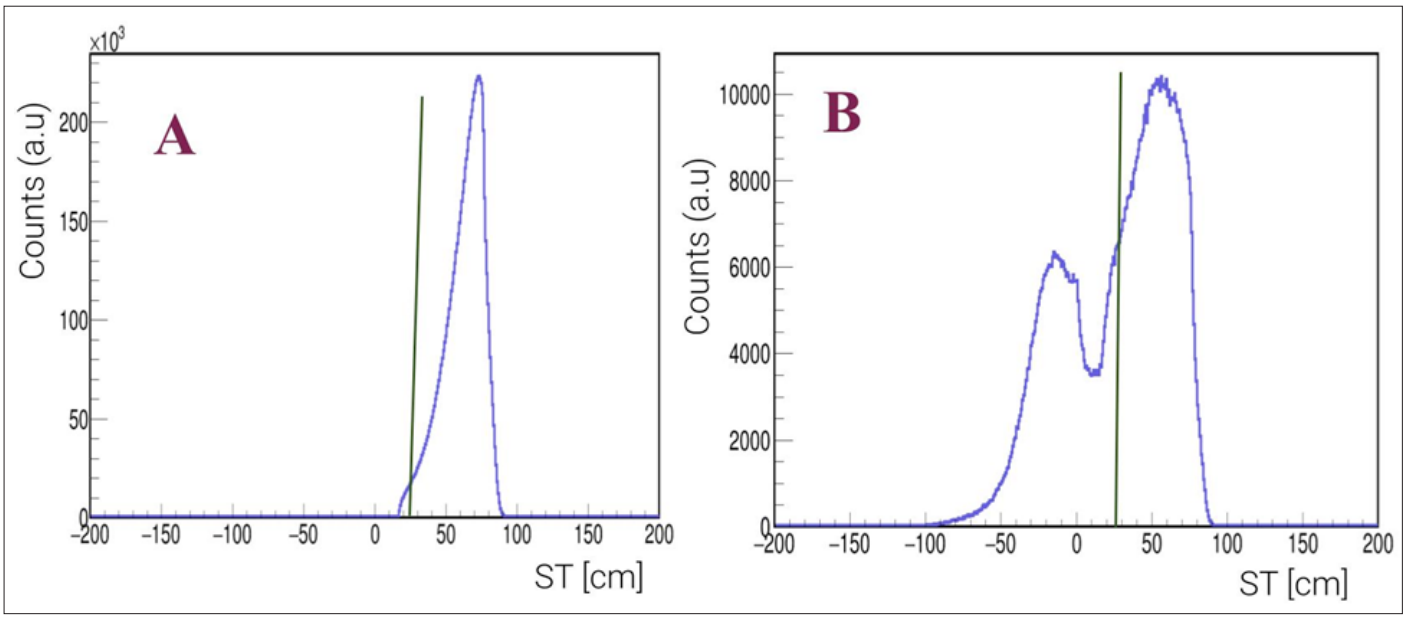

Fig. 7. Distribution of ST value, referred to as the scatter test. Figure A represents the two-hit-event case, while B corresponds to the three-hit-event case before introducing geometric cut.

as shown in the shaded region of Fig. 3. We focused on two- and three-hit events to select candidates for 2γ and 2γ + prompt gamma imaging.

The TOT spectra for two- and three-hit events are shown in Fig. 4. and 5., respectively. In these figures the first peak primarily identifies scattered events, which are not the main focus of our investigation. Our attention is drawn to the second enhancement, leading us to potential candidates for annihilation events, mainly associated with Compton scattering [30, 31]. We also considered the Compton edge, at higher TOT values, highlighting prospective candidates for deexcitation gamma emissions, as indicated in Fig. 5. The applied voltage thresholds were set at 30 mV and 70 mV.

The identification of annihilation photons based on the TOT range (indicated in Fig. 4. and 5.) may lead to the misclassification of the scattered photons as annihilation photons. The possible background events are shown in Fig. 6. We then imposed a spatial constraint by limiting the annihilation points to those within a 30-cm radius. This restriction ensured that only annihilation events occurring within a specific range were considered for analysis in both two- and three-hit scenarios. As a next step, we applied a scatter test for both 2γ and $\beta^+ + \gamma$ candidates. The test involved calculating the time difference $(t_1 - t_2)$ and distance between hits classified as originating from annihilation photons [32, 33]:

$$ST = D - c.|t_1 - t_2| \qquad (1)$$

Where c is the speed of light.

Fig. 6. below illustrates all possible types of scatters occurring in the detector for both two- and three-hit scenarios.

The scatter-test selection and histograms illustrating the scatter test for both double and triple coincidence cases are presented in Fig. 7A and 7B, respectively. For images following the scatter test, a threshold of 25 cm (indicated by the vertical line) is applied.

RESULTS AND DISCUSSION

The images presented in Fig. 8A. and 8B. result from selecting 2γ and 2γ + prompt events from the list mode of all detected events, as shown in Fig. 3. Fig. 8A. and 8B. show the distribution of annihilation points (direct image) after identifying annihilation photons and prompt gamma based on the TOT values (as shown in Fig. 4. and 5.).

In Fig. 8A., displaying images from two-hit events identified as 2γ annihilation, a ^{22}Na source is prominently visible at the centre, accompanied by the ring form of ^{68}Ge, situated away from the centre. In Fig. 8B., representing three-hit events with hits identified from two annihilation photons and prompt gammas, as expected, the ^{22}Na sodium source is visible and the ^{68}Ge ring is absent.

When superimposed on ^{22}Na and ^{68}Ge sources, this image also highlights instances of misidentified annihilation events due to scattering. The application of the $(t_1 - t_2)$ criterion and scatter test, as depicted in Fig. 7. with a threshold of 25 cm, significantly reduces scattering.

Our successful imaging of these two isotopes represents a milestone in simultaneously tracking and administering two tracers labelled with different radioisotopes and distinct biological molecules using the multiphoton J-PET scanner [1].

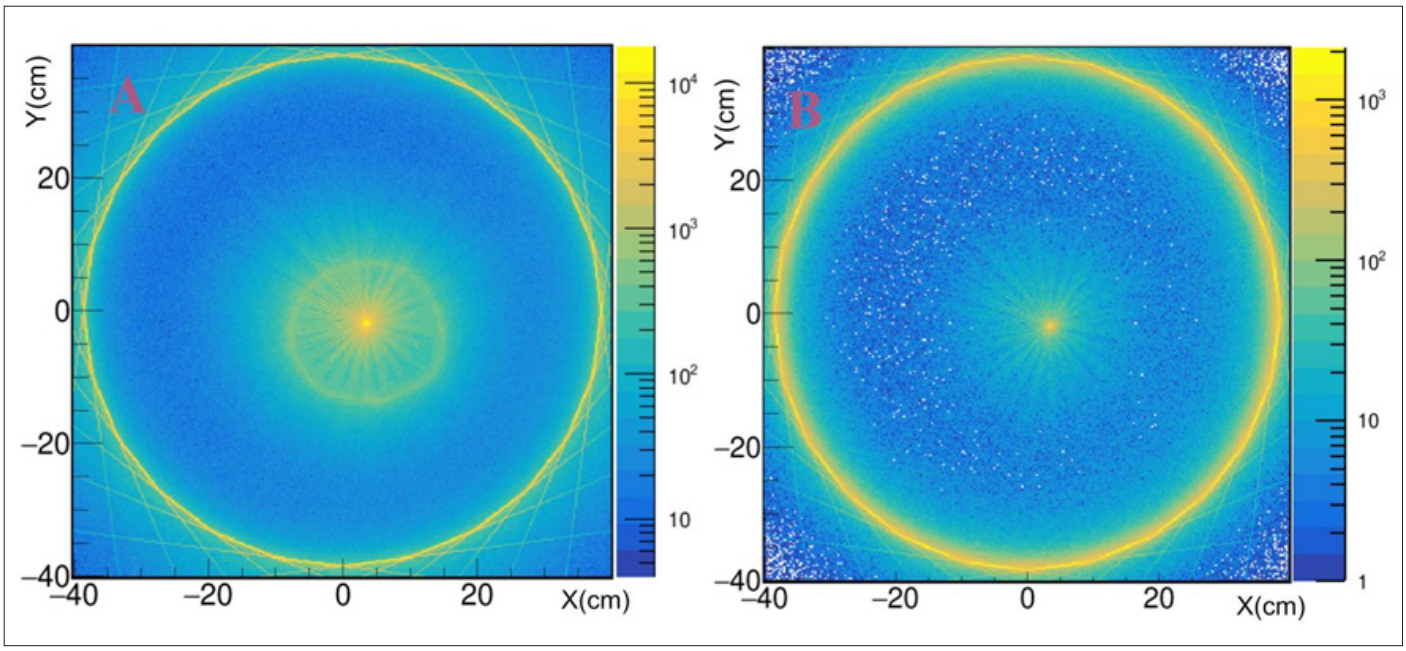

Fig. 8. Raw images from 2γ signals and three 2γ + deexcitation gamma signals. (A) Image reconstructed from two-hit events after applying TOT cuts (2.2 ns < TOT < 4.5 ns to 2200 ns * mV < TOT < 4500 ns); (B) Image reconstructed from three-hit events after applying TOT cuts (2200 ns < TOT < 4500 ns for annihilation and 4600 ns < TOT < 8800 ns for deexcitation gamma), as shown in Fig. 5. The outer ring with a diameter of about 76 cm is due to the scatterings of photons in the scintillator strips of the modular scanner.

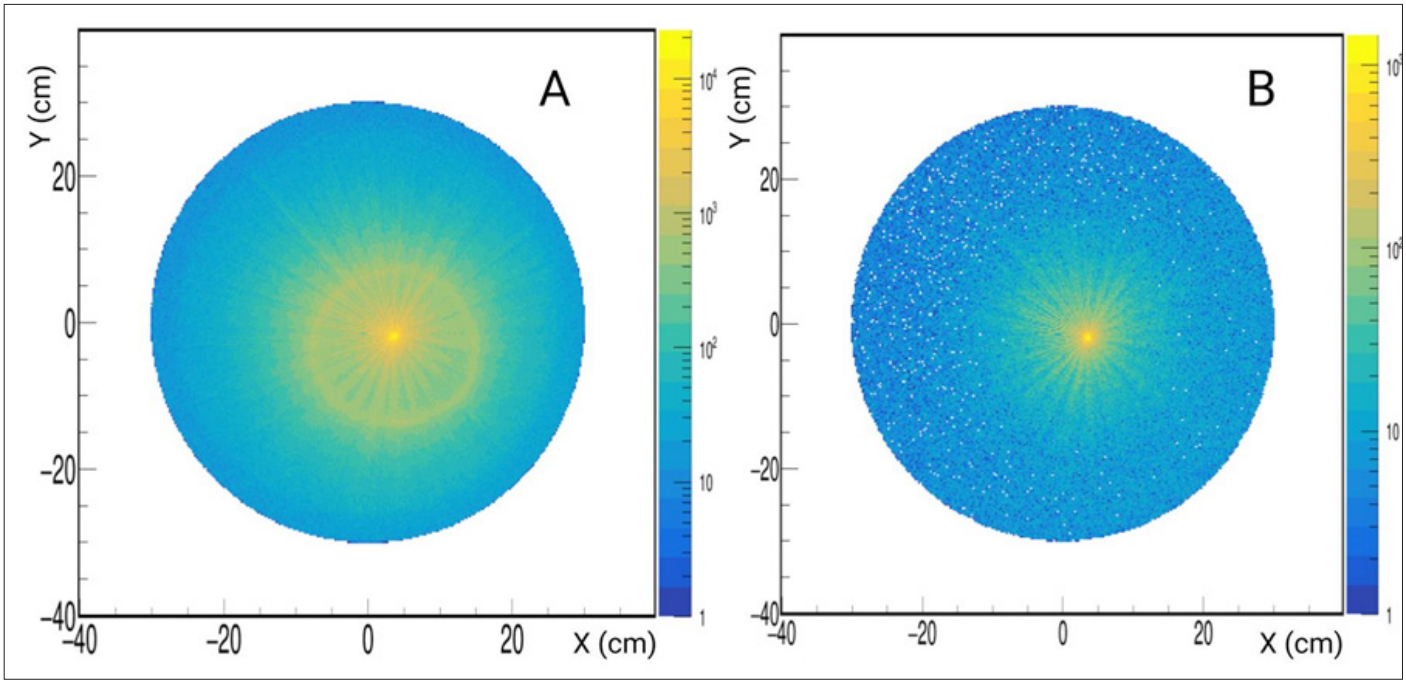

Fig. 9. Panel A displays the image obtained from double coincidence (showing signals from ^{22}Na and ^{68}Ge) events after the implementation of the scatter test. Panel B represents the resulting image after applying scatter test criteria to triple (β^+ + γ) coincidences in which only a signal from ^{22}Na is visible.

This innovative technique enables the concurrent tracking of multiple molecular targets and physiological processes in a single scan. This capability extends beyond ^{22}Na and ^{68}Ge isotopes, encompassing the potential for multi-tracer [1] and positronium imaging [6–8].

CONCLUSION

The study effectively demonstrates the feasibility and potential of simultaneous imaging with ^{22}Na and ^{68}Ge using the state-of-the-art modular J-PET scanner. The presented images in Fig. 8. and

9., derived from annihilation and deexcitation events, illustrate the capability of the J-PET scanner for simultaneous imaging of two distinct isotopes. Our analysis employed techniques, including TOT, TOF, and scatter test conditions, for both the 2γ and the $\beta^+ + \gamma$ coincidences.

Generally, our work represents a significant step towards harnessing the capabilities of the J-PET detector for dual--isotope imaging. Future efforts will address pending corrections for detection efficiency. The images in Fig. 8. and 9. constitute a preliminary step towards extracting images from ^{22}Na and ^{68}Ge sources. To isolate the image from ^{68}Ge it will be necessary to subtract an efficiency corrected three-hit image from the efficiency corrected two-hit image, with efficiency corrections currently in progress.

ACKNOWLEDGEMENTS

We acknowledge support from the Foundation for Polish Science through the TEAM POIR.04.04.00-00-4204/17 program, the National Science Centre of Poland through grant nos. 2021/42/A/ST2/00423 and 2021/43/B/ST2/02150, Jagiellonian University via project no. CRP/0641.221.2020, and the SciMat and qLife Priority Research Area budget, under the auspices of the Excellence Initiative – Research University at Jagiellonian University.

REFERENCES

1. Moskal P, Stępień E. Prospects and clinical perspectives of total body PET imaging using plastic scintillators. Pet Clin. 2020;15:439–52.
2. Moskal P, Niedźwiecki S, Bednarski T, Czerwiński E, Kubicz E, Moskal I, et al. Test of a single module of the J-PET scanner based on plastic scintillators. Nucl Instrum Methods Phys Res A. 2014;764:317-21.
3. Moskal P, Kowalski P, Shopa RY, Raczyński L, Baran J, Chug N, et al. Simulating NEMA characteristics of the modular total-body J-PET scanner—an economic total-body PET from plastic scintillators. Phys Med Biol. 2021;66(17):175015.
4. Niedźwiecki S, Białas P, Curceanu C, Czerwiński E, Dulski K, Gajos A, et al. J-PET: a new technology for whole-body PET imaging. Acta Phys Pol B. 2017;48:1567.
5. Korcyl G, Białas P, Curceanu C, Czerwiński E, Dulski K, Flak B, et al. Evaluation of single-chip, real-time tomographic data processing on FPGA SoC devices. IEEE Trans Med Imaging. 2018;37(11):2526-35.
6. Moskal P. Positronium Imaging. In: Proceedings of the IEEE Nuclear Science Symposium and Medical Imaging Conference; 2019 Nov; Manchester, England. New York: IEEE; 2019. p. 1, https://ieeexplore.ieee.org/document/9059856.
7. Moskal P, Dulski K, Chug N, Curceanu C, Czerwiński E, Dadgar M, et al. Positronium imaging with the novel multiphoton PET scanner. Sci. Adv. 2021;7(42):eabh4394.
8. Moskal P, Kisielewska D, Curceanu C, Czerwiński E, Dulski K, Gajos A, et al. Feasibility study of positronium imaging with the J-PET tomograph. Phys Med Biol. 2019;64(5):055017.
9. Moskal P, Kisielewska D, Shopa RY, Bura Z, Chhokar J, Curceanu C, et al. Performance assessment of the 2γ positronium imaging with the total--body PET scanners. EJNMMI Phys. 2020;7:1-16.
10. Moskal P, Jasińska B, Stępień EŁ, Bass SD. Positronium in medicine and biology. Nat Rev Phys. 2019;1(9):527-9.
11. Bass SD, Mariazzi S, Moskal P, Stępień E. Colloquium: Positronium physics and biomedical applications. Rev Mod Phys. 2023;95(2):021002.
12. Moskal P, Stępień EŁ. Perspectives on translation of positronium imaging into clinics. Front Phys. 2022;10:969806.
13. Moskal P, Gajos A, Mohammed M, Chhokar J, Chug N, Curceanu C, et al. Testing CPT symmetry in ortho-positronium decays with positronium annihilation tomography. Nat Commun. 2021;12(1):5658.
14. Pratt EC, Lopez-Montes A, Volpe A, Crowley MJ, Carter LM, Mittal V, et al. Simultaneous quantitative imaging of two PET radiotracers via the detection of positron–electron annihilation and prompt gamma emissions. Nat Biomed Eng. 2023;7(8):1028-39.
15. Fukuchi T, Shigeta M, Haba H, Mori D, Yokokita T, Komori Y, et al. Image reconstruction method for dual-isotope positron emission tomography. J Instrum. 2021;16(01):P01035.
16. Shimazoe K, Uenomachi M. Multi-molecule imaging and inter--molecular imaging in nuclear medicine. Bio-Algorithms Med Systems.2022;18(1):127-34.
17. Uenomachi M, Shimazoe K, Takahashi H. A double photon coincidence detection method for medical gamma-ray imaging. Bio-Algorithms Med-Systems. 2022;18(1):120-6.
18. Moskal P, Alfs D, Bednarski T, Białas P, Czerwiński E, Curceanu C, et al. Potential of the J-PET detector for studies of discrete symmetries in decays of positronium atom-a purely leptonic system. Acta Physica Polonica B. 2016;47(2): 509-35.
19. Brzezinski KW, Baran J, Borys D, Gajewski J, Chug N, Coussat A, et al. Detection of range shifts in proton beam therapy using the J-PET scanner: a patient simulation study. Phys Med Biol. 2023;68:145016.
20. Sharma S, Kacprzak K, Dulski K, Niedźwiecki S, Moskal P. Potential of modular J-PET for applications in the field of particle and medical physics. J Phys Conf Ser. 2022;2374(1):012040.
21. Sitarz M, Cussonneau JP, Matulewicz T, Haddad F. Radionuclide candidates for $\beta+ + \gamma$ coincidence PET: an overview. Appl Radiat Isot. 2020;155:108898.
22. Matulewicz T. Radioactive nuclei for $\beta+ + \gamma$ PET and theranostics: selected candidates. Bio-Algorithms Med-Systems. 2021;17(4):235-9.
23. Alavi A, Werner TJ, Stępień EŁ, Moskal P. Unparalleled and revolutionary impact of PET imaging on research and day-to-day practice of medicine. Bio-Algorithms Med Systems. 2021;17(4):203-12.
24. Stefaan V, Pawel M, Karp JS. State of the art in total body PET. EJNMMI Phys. 2020;7(1): 35.
25. Verger A, Kas A, Darcourt J, Guedj E. PET imaging in neuro-oncology: an update and overview of a rapidly growing area. Cancers. 2022;14(5):1103.
26. Cherry SR, Badawi RD, Karp JS, Moses WW, Price P, Jones T. Total-body imaging: transforming the role of positron emission tomography. Sci Transl Med. 2017;9(381):eaaf6169.
27. Conti M, Eriksson L. Physics of pure and non-pure positron emitters for PET: a review and a discussion. EJNMMI Phys. 2016;3:1-17.
28. Rakoczy K. Adaptation of image reconstruction algorithms with time--of-flight for the J-PET tomography scanner [master's thesis]. 2019.
29. Raczyński L, Wiślicki W, Krzemień W, Kowalski P, Alfs D, Bednarski T, et al. Calculation of the time resolution of the J-PET tomograph using kernel density estimation. Phys Med Biol. 2017;62(12):5076.

30. Sharma S, Chhokar J, Curceanu C, Czerwiński E, Dadgar M, Dulski K, et al. Estimating relationship between the time over threshold and energy loss by photons in plastic scintillators used in the J-PET scanner. EJNMMI Phys. 2020;7(1):1-15.

31. Sharma S, Baran J, Brusa RS, Caravita R, Chug N, Coussat A, et al. J-PET detection modules based on plastic scintillators for performing studies with positron and positronium beams. J Instrum. 2023;18(02):C02027.

32. Khalil MM. Positron Emission Tomography (PET): Physics and Instrumentation. In: Basic Sciences of Nuclear Medicine. Cham: Springer International Publishing; 2021, 289-318.

33. Kowalski P, Wiślicki W, Raczyński L, Alfs D, Bednarski T, Białas P, et al. Scatter fraction of the J-PET tomography scanner. Acta Phys Pol B. 2016;47:549-60.